International Journal of Heat and Mass Transfer 90 (2015) 505–514

Contents lists available at ScienceDirect

International Journal of Heat and Mass Transfer

journal homepage: www.elsevier.com/locate/ijhmt

Modelling the efficiency of a nanofluid direct absorption solar collector

V. Cregan, T.G. Myers *

Centre de Recerca Mathemàtica, Campus de Bellaterra Edifici C, 08193 Bellaterra, Barcelona, Spain

ARTICLE INFO

Article history:
Received 11 February 2015
Received in revised form 17 June 2015
Accepted 17 June 2015
Available online 13 July 2015

Keywords:
Nanofluid
Direct absorption solar collector
Solar energy
Efficiency

ABSTRACT

In this paper we present an approximate analytical solution to the steady state, two-dimensional model for the efficiency of an inclined nanofluid-based direct absorption solar collector. The model consists of a system of two differential equations; a radiative transport equation describing the propagation of solar radiation through the nanofluid and an energy equation. The heat source term is obtained via the radiative flux integral, which is highly non-linear with respect to wavelength due to the spectral-dependent fluid and nanoparticle indices of refraction and absorption. To make analytical progress we introduce an approximate power-law function for the radiative flux. Applying the method of separation of variables, the resulting solution is used to investigate the efficiency of the collector subject to variation in model parameters. In addition our approach allows for the inclusion of wavelength-dependent absorption and scattering due to both the base fluid and nanoparticles and also an approximation for reflectance and absorptance due to the collector and its associated surfaces.

1. Introduction

Solar energy has the capacity to solve one of the most significant needs facing modern society: namely the development of a sustainable and environmentally friendly energy source. One commonly-used form of solar energy capturing system is the solar thermal collector. Typically, a collector consists of a black surface used to absorb solar radiation. The solar energy is then transferred, as thermal energy, to a fluid running in tubes embedded or fused onto the surface of the collector. The two main factors affecting the efficiency of the collector are its absorption characteristics and the mechanism by which the heat is transferred to the fluid. Direct Absorption Solar Collectors (or DASCs) avoid heat transfer to the fluid by using the fluid itself to directly absorb the energy. However, due to their low absorptive properties, standard fluids are inefficient at absorbing solar radiation. One way to enhance absorption is to add solid particles to the fluid. This was recognised as early as the 1970's when micron-sized particles were added to fluids [1,22]. Unfortunately, the particles provided their own problems, such as clogging of pumps, settling out of solution and absorption of spectrums dominated by the base fluid. These problems were remedied with the advent of nanofluids in the mid-nineties [8]. Experimental research has demonstrated that dispersing trace amounts of nanoparticles into a base fluid can significantly enhance the chemical, optical and thermophysical properties of the fluid [9,10,13,26]. In comparison with fluids containing microparticles, nanofluids demonstrate improved stability, rheological properties and considerably higher thermal conductivities [20]. However, when describing the potential benefits of nanofluids one must be careful as in the past some of the claims regarding their enhanced properties have turned out to be questionable. For example, contradicting numerous experimental studies such as [11,12,15], the international benchmark study of Buongiorno et al. [7] suggested that there was no anomalous enhancement of thermal conductivity in the fluid. Furthermore, the analysis of MacDevette et al. [19] showed that the model derived in [6], and used by many researchers to show increased heat transfer coefficient, in fact leads to the opposite result. They go on to show that many previous erroneous results stem from 'ad hoc' assumptions or incorrect parameter values.

Nanofluid-based DASCs (NDASCs) exploit the nanofluid's optical and thermophysical properties to absorb and scatter solar radiation. Recent experimental and theoretical studies have shown that NDASCs have the potential to harness solar energy significantly more efficiently than traditional solar collectors, for example 10–30% increases in efficiency have been predicted [31,35]. From an economic perspective, theoretical research has shown that a 100 MW capacity solar energy thermal power tower could generate approximately $3.5 million more per year by including nanofluid technology [31]. At present NDASCs are not yet at an economically viable level of development [31]. To achieve this goal requires further experimental and theoretical research to optimise

* Corresponding author.

http://dx.doi.org/10.1016/j.ijheatmasstransfer.2015.06.055
0017-9310/

the effectiveness of the nanofluid in converting solar to thermal energy.

An immediate feature that emerges from the NDASC literature is the observed increase in collector efficiency with the addition of nanofluids when compared to traditional DASCs. Another characteristic is the sheer variety of nanoparticles and base fluids considered. Otanicar et al. [24] showed that the absorption properties of particle-free fluids were poor: water had the best absorption properties, absorbing 13% of the available solar energy. In a subsequent study, Otanicar et al. [25] constructed a nanofluid-based micro solar thermal-collector, and observed an initial rapid increase in efficiency with increasing particle volume fraction. However, when the volume fraction increased above a certain level the efficiency decreased slightly. Compared to particle-free fluids, their study demonstrated NDASC efficiency increases of approximately 20%. Taylor et al. [31] compared the performance of a nanofluid-based solar thermal system with a conventional one and showed that the use of nanofluids can increase efficiency by up to 10%. Yousefi et al. [35] observed a 28% increase in efficiency with the addition of a small amount of Al_2O_3 nanoparticles to water.

To date theoretical studies have typically focused on solving a steady state, two-dimensional system for a nanofluid enclosed between two parallel plates and flowing subject to a plug flow regime. The governing model consists of a system of two coupled differential equations; a radiative transport equation (hereafter referred to as RTE) describing the attenuation of solar radiation in the nanofluid and an energy equation for the temperature in the nanofluid. In general numerical simulations are required to solve the model, as the solution to the RTE involves a problematic wavelength-dependent integral for the radiative flux, which cannot be evaluated directly. The complexity of this integral varies depending on the model assumptions imposed. Tyagi et al. [33] used a numerical simulation of the model to consider the efficiency of an NDASC with a water and aluminium nanofluid. They observed improvements up to 80% in efficiency compared to conventional water-based collectors. Similarly, the numerical solution of Otanicar et al. [25] showed that the inclusion of 30 nm graphite nanoparticles in water-based, low-temperature (<100 °C) solar collectors yielded an approximate 23% increase in efficiency. The difference in efficiencies between the two works can be attributed to the fact that the model of Otanicar et al. [25] introduces additional effects which lead to a decrease in efficiency. These effects include the reflection due to the upper and lower panels of the collector, and the absorbance of the upper panel. In a related experimental and numerical study Taylor et al. [31] demonstrated 5–10% enhancements in efficiency for a high-temperature nanofluid-based concentrating thermal system. Taylor et al. [30] also considered nanofluid optical properties, and in particular the extinction coefficient. Their model did not agree with experimental results for some metallic nanoparticles, possibly due to impurities in the metals. Lenert and Wang [18] adopted a different approach by analysing a stationary nanofluid using a one-dimensional, time-dependent model. They considered collectors operating at high temperatures and thus thermal emission of the nanofluid is introduced into the model. The temporal aspect was included so that they could ascertain the optimal exposure time and temperature at which point a collector should be connected to a power generation cycle.

In contrast to the wealth of experiment and numerical studies, analytical treatments are rare in the literature, in large part due to the radiative flux integral. Thus, reduced models are typically used to study the qualitative behaviour of NDASCs. Veeraragavan et al. [34] derived an analytical solution via the method of eigenfunction expansions by excluding the effect of scattering due to the nanoparticles. In addition, they assumed constant nanoparticle optical properties and a non-absorbing base fluid. The latter of these assumptions is questionable as the bulk of the collector consists of the fluid medium, and hence it is expected that its radiative properties can have a significant impact on collector performance [29]. In the case of a Therminol VP-1-graphite nanofluid, their solution gave a maximum efficiency increase of 35%. Lee and Jang [17] simplified the model considerably by using constant optical properties and by applying a fixed initial spectral flux, rather than the commonly used black body relation. They demonstrated that for a water-based, multi-walled carbon nanotube NDASC, a small particle volume fraction of 0.012% can outperform a conventional solar flat plate collector by up to 20%.

In this paper, we consider the steady state, two-dimensional model for the efficiency of an NDASC in the low to mid-temperature range. In particular, we seek an analytical solution subject to an approximate expression for the heat source term. We use parameter values suitable for a water-based nanofluid containing aluminium particles as the thermophysical and wavelength-dependent optical properties of both are readily available. In general it is difficult to find the wavelength-dependent optical properties for other nanofluids. However, assuming one has the relevant data, our methodology is appropriate for a wide range of nanofluids.

To obtain an exact solution for the temperature profile, we apply several simplifying assumptions. Firstly, as in the case of previous studies [25,31,33,34], we presume a constant fluid velocity profile in the collector. We examine low particle volume fractions because if the particles are packed too close together, dependent and multiple scattering effects must be considered. Brewster and Tien [5,32] proposed that the independent scattering regime is only valid for nanofluids with particle concentrations lower than 0.6%. However, despite this restriction, effective NDASCs can still be obtained [30]. We focus on low to mid-temperature NDASCs so that we can neglect temperature-dependent thermal properties and nanofluid thermal radiation. Thus, the analysis is not applicable to high-temperature NDASCs. However, we note that for temperatures less than 750 K radiative emission constitutes a small fraction of the total radiative heat loss [34].

As discussed, the most challenging aspect of modelling NDASCs is deriving a closed-form expression for the radiative flux, due to the wavelength-dependent optical properties of both the base fluid and the nanoparticles. Our approach is to evaluate this integral numerically and then fit a power-law function to the numerical results. Next we take the gradient of the approximate flux expression to obtain the source term in the heat equation. The relatively simple form of the power-law function allows for an exact solution via separation of variables. The system parameters, and in particular the nanoparticle volume fraction, are then varied in the model to study their influence on collector performance. The main advantage of our method is that, unlike previous analytical studies [17,34], all of the wavelength-dependent optical properties are retained in the integral. Assuming constant optical properties is not always valid. For example, the index of absorption of water shows considerable variation with wavelength. In addition, absorption and scattering due to both the base fluid and nanoparticles are also easily included. We do not include the wavelength-dependent effects of absorptance and reflectance due to the upper glass panel and the lower surface of the collector as these prohibit an analytical solution. Instead, in Section 4 we propose an approximation for the combined effect of these factors.

The outline of this paper is as follows. In Section 2 the governing model is described. A description of the optical properties of the nanofluid and a derivation of the approximate heat source term is given in Section 2.1. In Section 3 the model is nondimensionalised and an analytical solution is presented. The results of the model are discussed in Section 4.

2. Mathematical model

A schematic of an NDASC is shown in Fig. 1. The nanofluid is confined within a channel of height H and length L. The fluid is enclosed at the top by a surface which is optically transparent, and thus permits the majority of the incident solar flux to pass into the nanofluid. The collector is inclined at an angle θ to the horizontal. As shown, (x^*, z^*) define a two-dimensional coordinate system aligned such that x^* is parallel to the channel base with $x^* = 0$ and $x^* = L$ at the collector inlet and outlet, respectively. The coordinate z^* is the perpendicular distance downwards from the upper surface with $z^* = 0$ and $z^* = H$ located at the top and base of the collector, respectively. The * notation denotes dimensional variables. The solar radiation striking the collector is absorbed by both the base fluid and the nanoparticles suspended in the fluid. The absorbed radiation leads to heat generation in the nanofluid. At the upper surface there is heat loss via convection and radiation, and this is modelled using a surface heat transfer coefficient. The base of the collector is assumed to be insulated. We adopt a similar approach to that of previous authors [25,33,34] and assume a velocity profile independent of x^* and z^*.

The particles and fluid are assumed to be at the same temperature, and hence the nanofluid is modelled as a single-phase isotropic fluid [18]. We assume that nanofluid properties such as density, heat capacity and thermal conductivity depend on the associated base fluid and nanoparticles properties, as well as the particle volume fraction, ϕ, but that they are independent of temperature.

From classical mixing theory the nanofluid density, ρ_{nf}, and specific heat capacity, $c_{p,nf}$, are

$$\rho_{nf} = \phi\rho_{np} + (1-\phi)\rho_{bf}, \quad c_{p,nf} = \frac{\phi\rho_{np}c_{p,np} + (1-\phi)\rho_{bf}c_{p,bf}}{\rho_{nf}}, \tag{2.1}$$

where the subscripts bf, np and nf denote base fluid, nanoparticle and nanofluid respectively. For the nanofluid thermal conductivity we use the expression of Myers et al. [23],

$$k_{nf} = \frac{k_{bf}}{(1-\phi^{1/3})^2}\left[(1-\phi) + \phi\frac{\rho_{np}c_{p,np}}{\rho_{bf}c_{p,bf}}\right]\frac{n-1}{2(n+1)}\left[\frac{1+\phi^{1/3}}{2} - \frac{1}{n+1}\right]^{-1}, \tag{2.2}$$

where $n = 2.233$. The above expression was shown to agree well with experimental data for several different nanofluids including water-aluminium. Unlike the classical conductivity model of Maxwell [21] for solid-in-liquid suspensions, (2.2) is based on the dynamic behaviour of a nanofluid on a finite domain, and hence is not limited to highly disperse fluids.

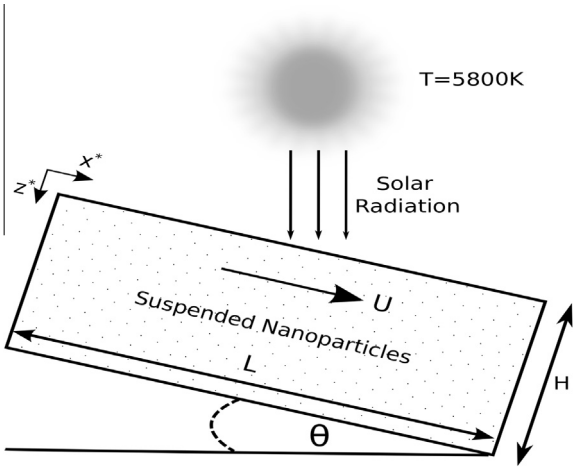

Fig. 1. Schematic of an inclined nanofluid-based direct absorption solar collector of length L and height H.

The energy equation governing the temperature in the nanofluid is

$$c_{p,nf}\rho_{nf}U\frac{\partial T^*}{\partial x^*} = k_{nf}\frac{\partial^2 T^*}{\partial z^{*2}} + q^*, \tag{2.3}$$

where T^* is the fluid temperature. The well-known solution for laminar, incompressible fluid flow down an inclined plane under the action of gravity (see [2]) is used to find an order of magnitude approximation for the constant nanofluid velocity in (2.3). The volume flux per unit width of the collector is

$$Q = \frac{\rho_{nf}g\sin\theta H^3}{12\mu_{nf}}, \tag{2.4}$$

which is used to give the average fluid velocity

$$U = \frac{Q}{H} = \frac{\rho_{nf}g\sin\theta H^2}{12\mu_{nf}}. \tag{2.5}$$

For the parameter values quoted in Table 2 and a practical inclination angle range of $[0, \frac{\pi}{4}]$, the maximum average velocity is approximately 0.8 m s^{-1}. The precise nature of the heat generation term, q^*, is discussed in detail in Section 2.1. We consider relatively low temperatures of the order 300 K, similar to those of Tyagi et al. [33], and hence, radiative emission is assumed negligible. This simplifies the model significantly as we can ignore the associated higher-order temperature terms associated with thermal radiation. However, as observed by Veeraragavan et al. [34], thermal emission in nanofluids accounts for only 5% of the total radiative heat loss for temperatures below 750 K, and thus our model is applicable to systems with higher temperatures. Another advantage of modelling low-temperature collectors is that we can assume that thermal properties are temperature-independent. The boundary condition at the surface panel is

$$k_{nf}\frac{\partial T^*}{\partial z^*}|_{z^*=0} = h_S\left(T^*|_{z^*=0} - T^*_{Amb}\right), \tag{2.6}$$

where T^*_{Amb} is the ambient temperature of the surrounding air. The surface heat transfer coefficient, h_S, depends on the material parameters of the upper surface. From [3], the overall heat transfer coefficient for a glass panel is given by

$$\frac{1}{h_S} = \frac{1}{h_A} + \frac{1}{h_W} + \frac{\Delta z}{k_G}, \tag{2.7}$$

where Δz is the panel thickness, $k_G \approx 1$W m^{-1} K^{-1} is the conductivity of glass, and h_A and h_W are the heat transfer coefficients between air and glass, and water, respectively. As h_W is typically much larger than h_A [28] and for a sufficiently thin panel $\Delta z/k_G \ll 1$, (2.7) reduces to $h_S \approx h_A$. To be consistent with the study of Tyagi et al. [33], we use $h_S = 6.43$ Wm^{-2} K^{-1}, which is of the same order of magnitude as the values obtained from the approximation of (2.7). The base of the collector is insulated, and hence we apply a zero flux boundary condition

$$\frac{\partial T^*}{\partial z^*}|_{z^*=H} = 0. \tag{2.8}$$

Finally, the fluid is assumed to be at a constant temperature, T^*_I, upon entering the collector, and thus the inlet condition is

$$T^*(0, z^*) = T^*_I. \tag{2.9}$$

2.1. Heat source term

The source term is obtained by an energy balance, whereby the change in the normally-incident solar spectral flux due to

attenuation of the nanofluid is dissipated as heat release. This energy balance is described by the one-dimensional radiative transport equation (RTE)

$$\frac{\partial J^*_\lambda}{\partial z^*} = -K_e J^*_\lambda, \tag{2.10}$$

where $J^*_\lambda(z^*, \lambda^*)$ is the spectral intensity and λ^* the wavelength. The nanofluid extinction coefficient, K_e accounts for light attenuation in the nanofluid due to the combined effects of absorption and scattering. As the temperatures in the collector are not expected to be overly high a temperature-dependent emission term in (2.10) has been neglected [18,33]. The boundary condition at the upper surface of the collector is the concentrated normal incident solar radiation, approximated by Planck's black body relation

$$J^*_\lambda(z^* = 0, \lambda^*) = J^*_{0\lambda}(\lambda^*) = \frac{2hc^2\Omega_S S_{Att}(1-R)}{\lambda^{*5}\left(\exp(\frac{hc}{\lambda^* k_B T_{Sun}}) - 1\right)} \tag{2.11}$$

where h is Planck's constant, c the speed of light, Ω_S the solid angle of the sun, k_B is the Boltzmann constant and T_{Sun} is the temperature of the sun. The (to be determined) attenuation constant, S_{Att}, accounts for the attenuation of sunlight through the Earth's atmosphere. The fixed parameter R is an approximation for the reflectance in the collector due to reflectance and absorptance in the collector. In Section 4 we will highlight relevant experimental work that suggests an approximate value of R.

The solution to (2.10), subject to (2.11), is

$$J^*_\lambda(z^*, \lambda^*) = J^*_{0\lambda} e^{-K_e z^*}, \tag{2.12}$$

which demonstrates that the spectral intensity is a decreasing function of the light path z^*. An RTE exists for each wavelength, and thus to determine the radiative flux, $P^*(z^*)$, (2.12) must be integrated over the entire spectrum to give

$$P^*(z^*) = \int_0^\infty J^*_\lambda(z^*, \lambda^*)\,\mathrm{d}\lambda^* = \int_0^\infty J^*_{0\lambda} e^{-K_e z^*}\,\mathrm{d}\lambda^*. \tag{2.13}$$

The nanofluid extinction coefficient is

$$K_e = K_a^{bf} + K_s^{bf} + K_a^{np} + K_s^{np}, \tag{2.14}$$

where the subscripts a and s denote absorption and scattering, respectively. In combining the base fluid and nanoparticle contributions in (2.14), we assume independent scattering [5,32], such that the scattered radiation in the nanofluid do not interact with each other, and thus the intensities may be added.

The bulk of the volumetric receiver consists of the fluid medium, and hence the radiative properties of the fluid have a non-negligible effect on receiver performance [29]. Taylor et al. [30] observe that for fluid depths of the order 10 cm, of the energy absorbed, nanoparticles absorb 65% to 70% of the incoming solar energy, with the base fluid absorbing approximately 30%. For pure fluids, light scattering is negligible, and only the attenuation due to absorption need be considered [16]. Hence, the spectral absorption and scattering coefficients for the base fluid are

$$K_a^{bf} = \frac{4\pi\kappa_a^{bf}}{\lambda^*}, \quad K_s^{bf} \approx 0, \tag{2.15}$$

where κ_a^{bf} is the fluid index of absorption.

For nanofluids the presence of small particles gives rise to more complex absorption and scattering spectral coefficients. The wavelength of solar radiation is greater than 250 nm, and is thus at least ten times larger than the mean diameter of typical NDASC nanoparticles (<50 nm). Hence, the higher order spectral components associated with Mie scattering theory may be neglected, and the Rayleigh scattering approximation is applicable [30]. The extinction coefficient for a spherical nanoparticle is

$$K_a^{np} + K_s^{np} = \frac{3\phi}{2D}(Q_a^{np} + Q_s^{np}), \tag{2.16}$$

where D is the diameter of the particles. From [29,30,33], the nanoparticle absorption and scattering efficiencies are

$$Q_a^{np} = 4\alpha \mathrm{Im}\left\{\frac{m^2-1}{m^2+2}\left[1 + \frac{\alpha^2}{15}\left(\frac{m^2-1}{m^2+2}\right)\frac{m^4+27m^2+38}{2m^2+3}\right]\right\},$$
$$Q_s^{np} = \frac{8}{3}\alpha^4\left|\frac{m^2-1}{m^2+1}\right|^2, \tag{2.17}$$

where $m = (n_{np} + i\kappa_a^{np})/n_{bf}$ is the relative complex refractive index of the particles to the fluid. The refractive indices n_{bf} and n_{np} and the nanoparticle absorption index κ_a^{np} may be found in [4,27]. The size parameter is defined as $\alpha = (\pi D)/\lambda^*$, and in the Rayleigh scattering regime we require $\alpha \ll 1$ and $|m|\alpha \ll 1$. A cursory glance at (2.17) reveals that $Q_a^{np} \sim \mathcal{O}(\alpha)$ and $Q_s^{np} \sim \mathcal{O}(\alpha^4)$, and thus for particles with small diameter scattering effects are much smaller than absorption effects. Veeraragavan et al. [34] neglect the scattering term completely. Other studies [25,33] retain scattering since it does not make the analysis any more complex, and makes clear the impact of particle diameter. Hence we will also retain the scattering term. Substituting (2.17) into (2.16) yields

$$K_e^{np} = \frac{6\pi}{\lambda^*}\phi \mathrm{Im}\left[\frac{m^2-1}{m^2+2}\left[1 + \frac{\alpha^2}{15}\left(\frac{m^2-1}{m^2+2}\right)\frac{m^4+27m^2+38}{2m^2+3}\right]\right] + \frac{4\pi^4 D^3}{\lambda^{*4}}\phi\left|\frac{m^2-1}{m^2+1}\right|^2. \tag{2.18}$$

Then substituting (2.11) into (2.13) leads to the radiative flux integral

$$P^*(z^*) = C_0 \int_0^\infty \frac{(1-R)\exp(-K_e z^*)}{\lambda^{*5}[\exp(\frac{C_1}{\lambda^*}) - 1]}\,\mathrm{d}\lambda^*, \tag{2.19}$$

where K_e is defined by (2.14), $C_0 = 2hc^2\Omega_S S_{Att}$ and $C_1 = (hc)/(k_b T_{Sun})$.

Before the radiative flux integral (2.19) can be evaluated, several parameters must be fixed. To be consistent with previous treatments [33,34] we require the incident solar flux at the upper surface of the collector to be $G_S = 1000\,\mathrm{W\,m^{-2}}$ (i.e. $P(0) = G_S$). Setting $z = 0$ in (2.19) and solving the integral numerically, yields $S_{Att} \approx 0.7$.

The indices of refraction and absorption are wavelength-dependent, and in practice (2.19) cannot be evaluated directly. Lee and Jang [17] simplify the integral considerably by assuming a wavelength independent integrand. Veeraragavan et al. [34] neglect reflectance, assume that absorption due to the fluid is negligible, and the remaining optical properties are constant, and thus (2.19) can be integrated exactly to give

$$P^*(z^*) = \frac{C_0}{C_1^4}\psi_3\left(1 + \frac{6\pi K_1}{C_1}\phi\frac{z^*}{H}\right), \tag{2.20}$$

where ψ_3 is the polygamma function of order 3 and $K_1 = \mathrm{Im}\{(m^2-1)/(m^2+2)\}$.

We wish to retain the wavelength-dependent properties in the model, and hence apply a combined numerical-analytical approach to evaluate the radiative flux. Firstly, (2.19) is calculated numerically via the trapezoidal rule in the range $z^* \in [0, H]$ for a given ϕ. A power-law function that decays with z^* is then fitted to the numerical values via a nonlinear least squares fitting routine in Matlab. The approximating function takes the form

$$P_f^*(z^*) = \frac{G_S}{\left(1 + \beta_0 \frac{z^*}{H}\right)^{\beta_1}}, \tag{2.21}$$

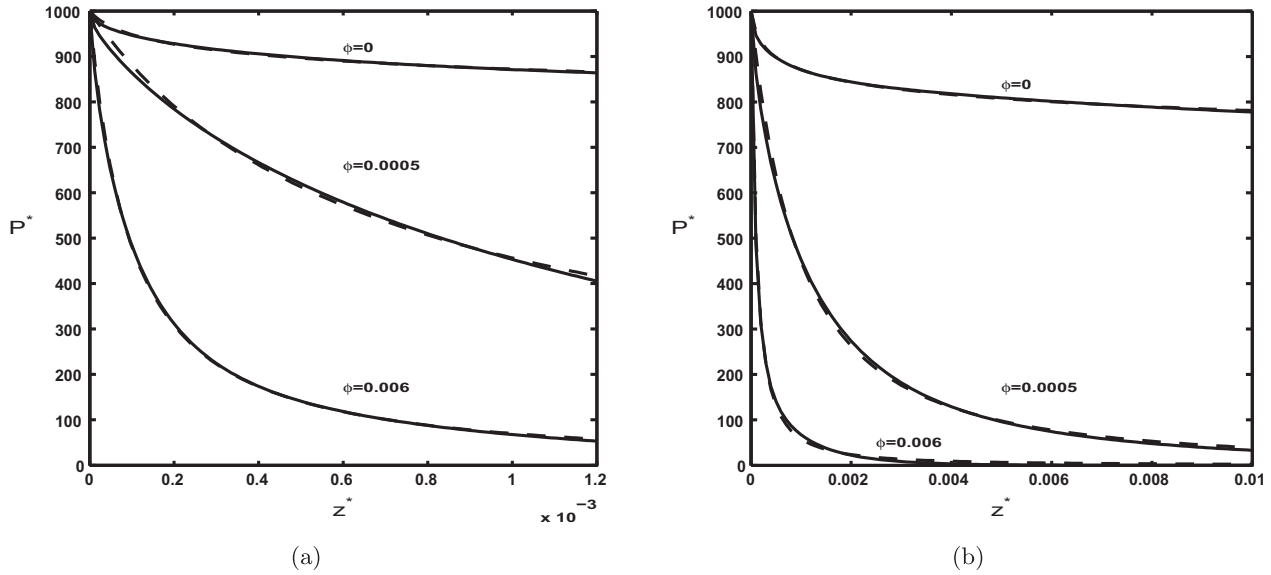

Fig. 2. Comparison of numerical solution for radiative flux (solid line) with power-law fit (dashed line) for $\phi = 0, 0.0005, 0.006$ for a water-aluminium nanofluid, for (a) $H = 1.2$ mm and (b) $H = 1$ cm. $D = 20$ nm and $R = 0$.

where the dimensionless parameters β_0 and β_1 depend on ϕ, H and the optical parameters of the nanofluid. The heat source term is given by the derivative of the radiative flux:

$$q^* = -\frac{dP_f^*}{dz^*} = \frac{G_S\beta_0\beta_1}{H(1+\beta_0\frac{z^*}{H})^{\beta_1+1}}. \tag{2.22}$$

Fig. 2 compares the numerical integration of (2.19) (solid lines) with the power-law approximation (2.21) (dashed lines) for various particle volume fractions and channel heights. In the case of a collector with channel height 1.2 mm, the values of (β_0, β_1) used in the $\phi = 0, 0.0005, 0.006$ power-law approximations are $(31, 0.04), (2.30, 0.74)$ and $(10.60, 1.14)$, respectively. Similarly, for a collector with height 1 cm the (β_0, β_1) values are $(158.12, 0.05), (6.51, 1.61)$ and $(56.02, 1.51)$. Except for a small region near $z = 0$ the pairs of curves in Fig. 2 are almost indistinguishable. The graphs demonstrate two obvious physical features. Firstly, $P^*(z^*)$ decreases with increasing fluid depth due to the attenuation in solar radiation. Secondly, the inclusion of nanoparticles leads to a significant increase in the energy absorbed by the fluid. Fig. 3 shows the variation of β_0 and β_1 with ϕ for the two aforementioned channel heights. Both parameters change rapidly near $\phi = 0$, i.e, the transition from a particle-free fluid to a nanofluid with small ϕ. For larger ϕ values, $\phi > 10^{-3}$, β_0 increases monotonically whilst β_1 remains $\mathcal{O}(1)$.

To clarify the contribution of each component, in Fig. 4 we present values of $P^*(z^*)$ for the base fluid (dash-dotted), nanoparticles (dashed) and nanofluid (solid) for ϕ equal to 0.0005 and 0.006. In both figures the nanoparticle curve is much closer to that of the nanofluid than the associated base fluid curve. This indicates that the nanoparticles make the greatest contribution to the overall nanofluid radiative flux. However, the base fluid clearly also makes a non-negligible contribution, and so should be included in any analysis of nanofluid absorbance.

3. Solution method

The mathematical model is described by the heat Eq. (2.3), with the source term specified by expression (2.22) and the average fluid velocity U by (2.5),

$$c_{p,nf}\rho_{nf}U\frac{\partial T^*}{\partial x^*} = k_{nf}\frac{\partial^2 T^*}{\partial z^{*2}} + \frac{G_S\beta_0\beta_1}{H(1+\beta_0\frac{z^*}{H})^{\beta_1+1}}. \tag{3.1}$$

We define the dimensionless variables

$$x^* = Lx, \quad z^* = Hz, \quad T^* = \Delta T.T + T_I^*, \tag{3.2}$$

where the temperature scale ΔT is as yet unknown. Substituting (3.2) into (3.1) and rearranging yields

$$\frac{\partial T}{\partial x} = \gamma\frac{\partial^2 T}{\partial z^2} + \frac{G_S\beta_0\beta_1 H}{k_{p,nf}\Delta T(1+\beta_0 z)^{\beta_1+1}}, \tag{3.3}$$

where $\gamma = (k_{nf}L)/(\rho_{nf}c_{p,nf}UH^2)$. The temperature variation in the nanofluid is driven by the source term and hence the temperature scale is chosen to be

$$\Delta T = \frac{G_S L\beta_0\beta_1}{H\rho_{nf}c_{p,nf}U}, \tag{3.4}$$

which leads to

$$\frac{\partial T}{\partial x} = \gamma\frac{\partial^2 T}{\partial z^2} + \frac{1}{(1+\beta_0 z)^{\beta_1+1}}. \tag{3.5}$$

The scaled boundary conditions are

$$\left.\frac{\partial T}{\partial z}\right|_{z=0} = \mathrm{Nu}\left(T|_{z=0} - \widehat{T}\right), \quad \left.\frac{\partial T}{\partial z}\right|_{z=1} = 0, \quad T(0,z) = 0, \tag{3.6}$$

where $\widehat{T} = (T_{Amb}^* - T_I^*)/\Delta T$. The dimensionless Nusselt number, $\mathrm{Nu} = (Hh_S)/k_{nf}$, is the ratio of convective to conductive heat transfer at the upper panel.

The dimensionless formulation makes clear the factors affecting the temperature profile. Five nondimensional groupings appear: β_0, β_1 which describe the heat input; γ, which reflects the importance of conduction to advection; $\widehat{T}$ and Nu which reflect the cooling effect. As can be seen in the solution below, these all play an important role in determining the temperature profile.

Eqs. (3.5) and (3.6) may be solved by the method of separation of variables. The presence of nonhomogeneous terms in the system suggests a solution of the form $T(x,z) = v(x,z) + w(z)$ leading to

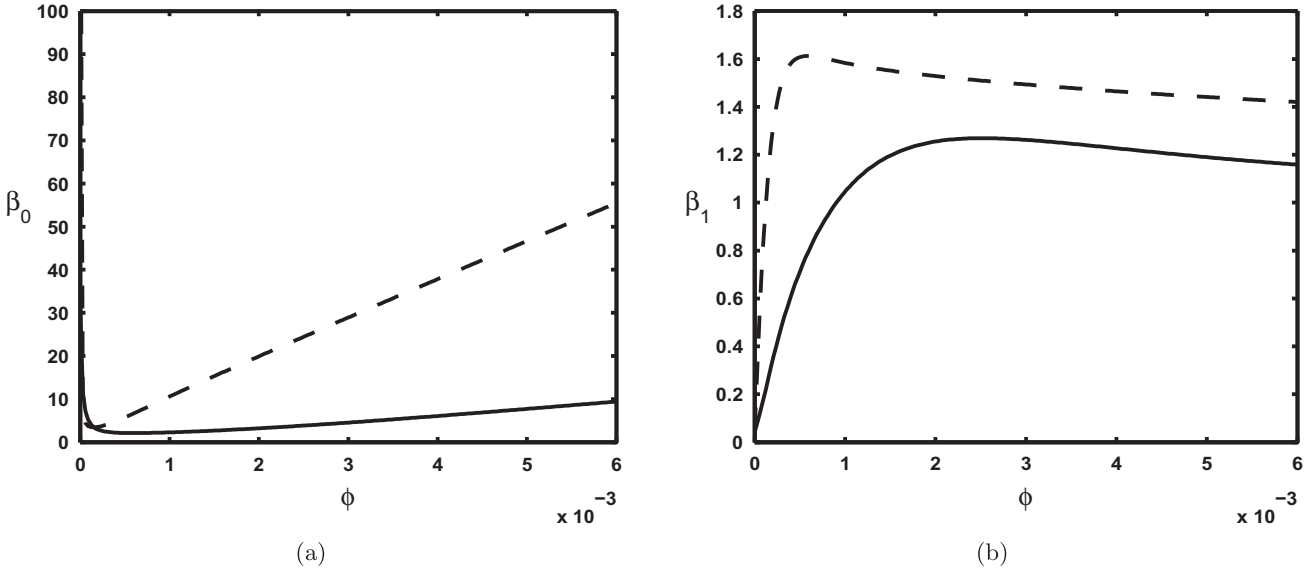

Fig. 3. Variation of (a) β_0 and (b) β_1 with ϕ for $H = 1.2$ mm (solid lines) and $H = 1$ cm (dashed lines).

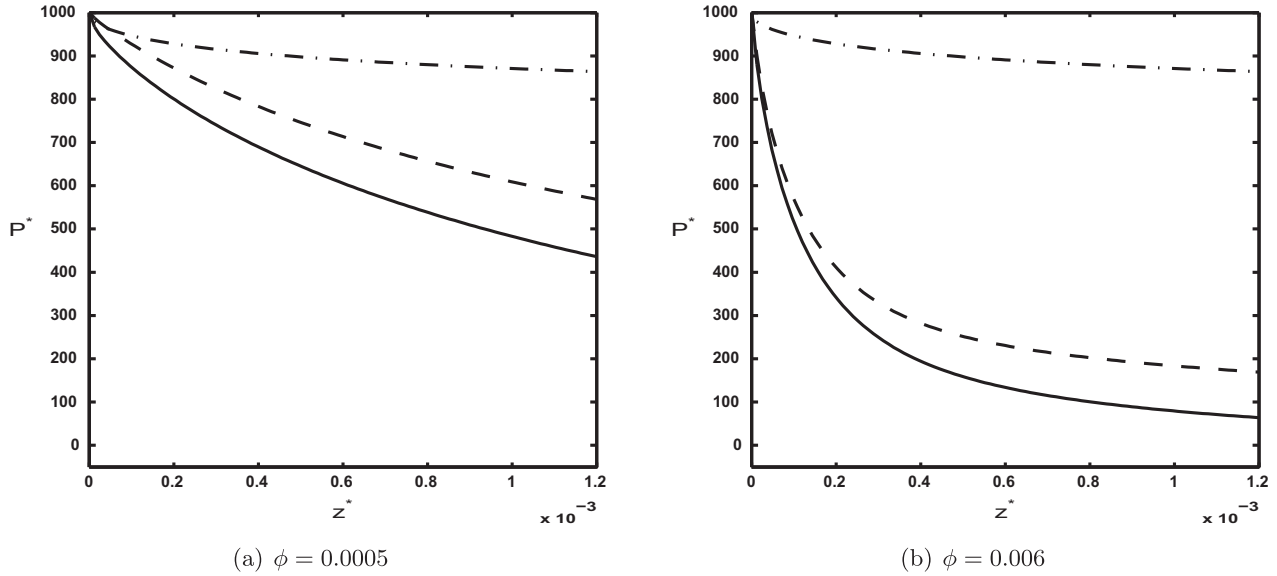

Fig. 4. Radiative flux contribution of base fluid (dash-dotted), nanoparticles (dashed) and nanofluid (solid) for a water-aluminium nanofluid for ϕ equal to (a) 0.0005 and (b) 0.006, $H = 1.2$ mm, $D = 20$ nm and $R = 0$.

$$T(x,z) = \sum_{n=1}^{\infty} D_n \exp(-\gamma p_n^2 x)\left(\cos(p_n z) + \frac{\mathrm{Nu}}{p_n}\sin(p_n z)\right) + w(z), \tag{3.7}$$

where the eigenvalues p_n satisfy

$$p_n \tan p_n - \mathrm{Nu} = 0, \tag{3.8}$$

and the integration constant is given by

$$D_n = -\frac{\int_0^1 w(z)(\cos(p_n z) + \frac{\mathrm{Nu}}{p_n}\sin(p_n z))\,\mathrm{d}z}{\int_0^1 (\cos(p_n z) + \frac{\mathrm{Nu}}{p_n}\sin(p_n z))^2\,\mathrm{d}z}. \tag{3.9}$$

The solution to the nonhomogeneous component in (3.7) is

$$w(z) = -\frac{1}{\gamma\beta_0^2\beta_1(\beta_1-1)(1+\beta_0 z)^{\beta_1-1}} + A_1 z + A_2, \tag{3.10}$$

where the boundary conditions are used to determine

$$A_1 = -\frac{1}{\gamma\beta_0\beta_1(1+\beta_0)^{\beta_1}},\quad A_2 = \frac{1}{\mathrm{Nu}}\left(\frac{1}{\gamma\beta_0\beta_1} + A_1\right) + \frac{1}{\gamma\beta_0^2\beta_1(\beta_1-1)} + \widehat{T}. \tag{3.11}$$

4. Results

In this section, the results of the model are discussed. Parameter values appropriate for a water-aluminium nanofluid were used. Table 1 lists the thermophysical properties of the nanofluid and Table 2 summarises the physical constants and collector parameters. Unless stated otherwise, the collector parameters are taken from Tyagi et al. [33]. The particle volume fractions used in the discussion are less than 0.006 (or 0.6%) so that the independent scattering assumption is not violated. The approximate reflectance R was assigned by comparing our model with the experimental study of Otanicar et al. [25]. In the independent scattering regime

Table 1
Thermophysical parameters of water and aluminium.

Substance	ρ_{bf}, ρ_{np} (kg/m^3)	k_{bf}, k_{np} (W/m K)	$c_{p,bf}, c_{p,np}$ (J/kg K)
Water	1000	0.609	4187
Aluminium	2700	247	900

Table 2
Collector parameters and physical constants.

Quantity	Symbol	Value	Units
Collector length/width/height	$L/W/H$	1, 1, 0.0012	m
Collector angle of inclination	θ	$\pi/9$	–
Viscosity (H_2O)	μ_{bf}	10^{-3}	kg m^{-1} s^{-1}
Surface heat transfer coefficient	h_S	6.43	W m^{-2} K^{-1}
Air/inlet nanofluid temperature	T^*_{Amb}/T^*_I	298.15/308.15	K
Temperature of the sun	T_{Sun}	5800	K
Incident solar radiation	G_S	1000	W m^{-2}
Solid angle of the sun	Ω_S	6.8×10^{-5}	–
Gravity	g	9.8	m s^{-2}
Speed of light	c	299792458	m s^{-1}
Boltzmann constant	k_b	1.38×10^{-23}	kg m^2 s^{-2} K^{-1}
Planck's constant	h	6.63×10^{-34}	kg m^2 s^{-1}

(i.e., $\phi < 0.006$) they obtained maximum efficiencies of the order 50% for several different nanofluids. We may obtain a similar level of efficiency as in Otanicar et al. [25] by simply choosing $R = 0.35$. Initially, we consider the nanofluid temperature in the collector subject to normal operating conditions. Then we study the performance of the collector due to variations in system parameters such as the particle volume fraction, particle diameter, channel height and inclination angle. Collector performance is typically evaluated via the well-known efficiency parameter, which is the ratio of usable thermal energy to incident solar energy. From [25,33] the standard efficiency expression used in the study of the steady state, two-dimensional model is

$$\eta = \frac{\dot{m} c_{p,nf}(\overline{T}^*_O - T^*_I)}{G_S A}, \tag{4.1}$$

where $\dot{m}$ is the mass flow rate of the fluid flowing through the collector, $\overline{T}^*_O$ is the mean fluid outlet temperature and A is the top surface area of the collector. Note, although the calculations of [25,33] are two-dimensional, the above formula corresponds to a three-dimensional result. This is obtained by calculating the mass flow rate per unit width in two-dimensions and then multiplying the top and bottom of the two-dimensional efficiency expression by the collector width, resulting in (4.1). In reality the mass flow rate obtained via a three-dimensional calculation differs from the two-dimensional version multiplied by the width, due to wall effects. Consequently, we will employ the correct two-dimensional version, which neglects the collector walls. Noting that the mass flux per unit width is given by the expression for Q of Eq. (2.4).

$$\eta = \frac{(\rho_{nf} Q) c_{p,nf}(\overline{T}^*_O - T^*_I)}{G_S L} = \frac{\rho_{nf} U H c_{p,nf}(\overline{T}^*_O - T^*_I)}{G_S L}, \tag{4.2}$$

where U is the average velocity given by (2.5). We note that via (3.2) and (3.4), (4.2) reduces further to

$$\eta = \beta_0 \beta_1 \overline{T}_O, \tag{4.3}$$

where $\overline{T}_O$ is the dimensionless outlet temperature.

Fig. 5 shows the temperature profile predicted by Eq. (3.7) as a function of depth at various points along the length of the collector for two values of volume fraction $\phi = 0.0005, 0.006$. Obviously the effect of radiation is greatest near the surface, $z = 0$, leading to higher temperatures there. The slight decrease in the immediate vicinity of $z = 0$ is due to the heat transfer to the collector surface. The strength of this decrease is related to the Nusselt number $\mathrm{Nu} = (Hh_S)/k_{nf}$ and ambient temperature: a larger Nu or lower ambient temperature will act to decrease the surface temperature further. As the fluid moves down the collector, increasing x, the temperature increases. With $\phi = 0.0005$ the difference in temperature between the top and bottom of the fluid is relatively small. With the higher volume fraction $\phi = 0.006$ temperatures are higher, as expected, but more energy is absorbed near the surface leading to a greater temperature gradient through the fluid depth. Inspection of the temperature scale in (3.4) suggests how the model parameters influence the nanofluid temperature. For example, the collector length, L, is proportional to ΔT, and thus one would expect higher temperatures for longer collectors. In addition, $\rho_{nf}, c_{p,nf}, \beta_0, \beta_1$ and U are functions of ϕ, and thus ϕ can be adjusted to attain higher temperatures.

The goal of this work is to improve collector efficiency, which is proportional to the outlet temperature. The exponential decay term in series solutions of the form (3.7) indicates that sufficiently far from

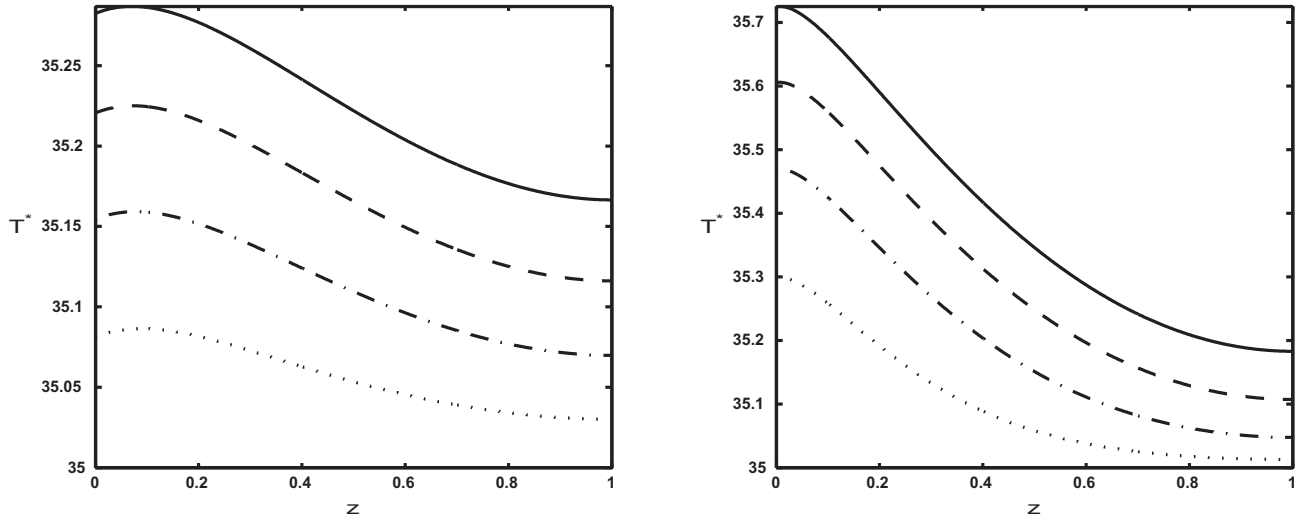

(a) $\phi = 0.0005$ (b) $\phi = 0.006$

Fig. 5. Temperature profiles for a water-aluminium nanofluid at $x^* = 0.25L$ (dotted line), $x^* = 0.5L$ (dash-dotted line), $x^* = 0.75L$ (dashed line) and $x^* = L$ (solid line) for (a) $\phi = 0.0005$ and (b) $\phi = 0.006$. $H = 1.2$ mm, $\theta = \pi/9$ and $D = 20$ nm.

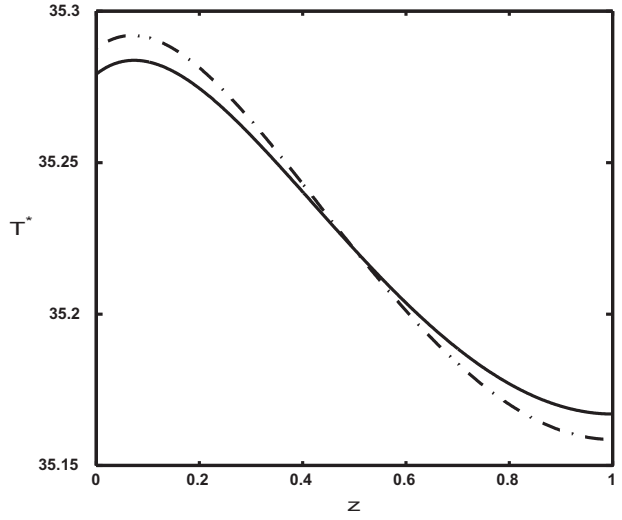

(a) $\phi = 0.0005$

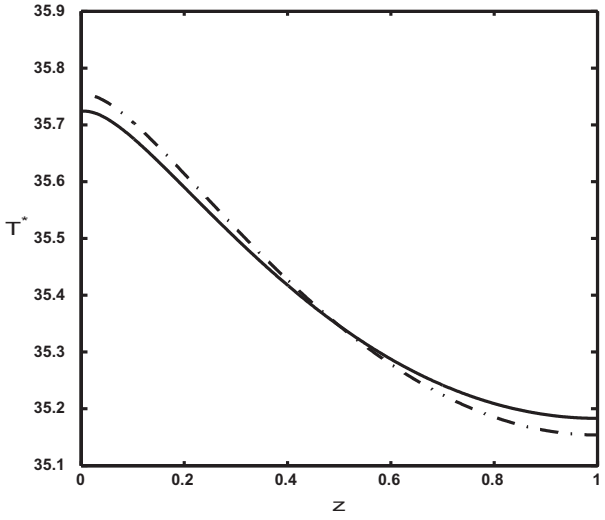

(b) $\phi = 0.006$

Fig. 6. Temperature profile at $x = 1$ using ten terms (solid line) and one term (dash-dotted line) in series solution (3.7) for (a) $\phi = 0.0005$ and (b) $\phi = 0.006$. $H = 1.2$ mm, $\theta = \pi/9$ and $D = 20$ nm.

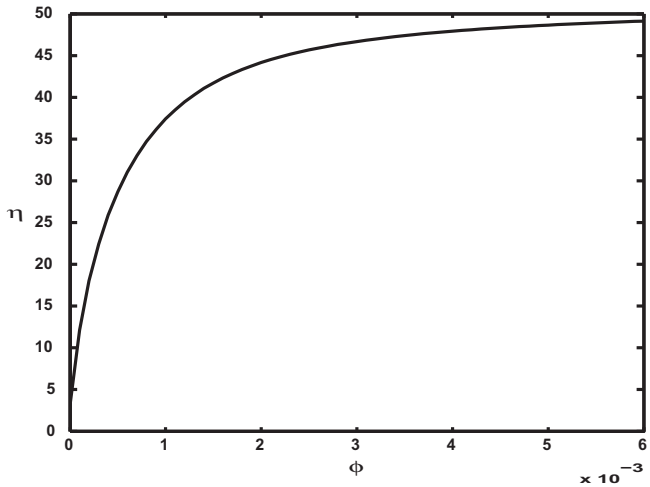

Fig. 7. Collector efficiency as a function of particle volume fraction for $R = 0.35, H = 1.2$ mm, $\theta = \pi/9$ and $D = 20$ nm.

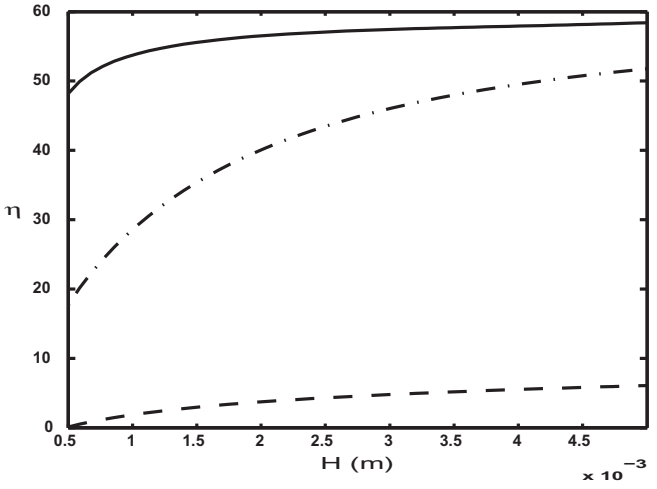

Fig. 8. Collector efficiency as a function of collector height for $\phi = 0$ (dashed line), $\phi = 0.0005$ (dash-dotted line) and $\phi = 0.006$ (solid line). $D = 20$ nm and $R = 0.35$.

the inlet only the first term in the series is significant. Moreover, over the practical particle volume fraction range, for collectors with channel heights of 1 mm and 1 cm, Nu is $\mathcal{O}(10^{-2})$ and $\mathcal{O}(10^{-1})$, respectively. Thus, since $\mathrm{Nu} \ll 1$ the eigenvalue $p_1 \approx \sqrt{\mathrm{Nu}}$. As a consequence we consider the reduced one term solution

$$T(x,z) \approx D_1 \exp(-\gamma \mathrm{Nu} x)\left(\cos(\sqrt{\mathrm{Nu}}z) + \sqrt{\mathrm{Nu}}\sin(\sqrt{\mathrm{Nu}}z)\right) + w(z). \tag{4.4}$$

In Fig. 6 we compare the one term solution (dashed line) with a ten term solution (solid line). Obviously the agreement is reasonable, and it will improve with increasing values of γ, for example with longer collectors or slower flows. A simplified solution could then be obtained by using just this first term in the series.

In Fig. 7 we present the variation of efficiency with volume fraction for $R = 0.35, H = 1.2$ mm, $\theta = \pi/9$ and $D = 20$ nm. For very small ϕ the efficiency rapidly increases. However, as ϕ increases the rate of increase in efficiency begins to slows down. This is a consequence of the exponential variation of spectral intensity with ϕ, see Eq. (2.12). For water-based nanofluids containing graphite nanoparticles and carbon nanotubes, the combined experimental and numerical study of Otanicar et al. [25] (which includes reflectance) leads to a similar result to that in Fig. 7. The numerical simulation of Tyagi et al. [33] neglects the effects of reflectance, and hence in the range $\phi \in [0, 0.005]$ they obtain efficiencies much higher than those reported here. As discussed, our choice of reflectance is based on the order of magnitude of the results of Otanicar et al. [25]. A smaller value of R would bring our solutions closer to the higher efficiency levels predicted in [17,33] where reflectance was neglected. We note that the value of R only affects the magnitude of the efficiency, and not the overall qualitative behaviour.

The curves in Fig. 8 illustrate the relationship between the channel height, H and the efficiency, η for a particle-free fluid and two nanofluids with particle volume fractions of 0.0005 and 0.006. In the case of the latter two, they exhibit similar behaviour to that outlined in Fig. 7. The relationship between H and η is explained as follows. As light passes through the channel the spectral intensity decreases via fluid attenuation. For fluids enclosed in deeper channels, the attenuation will be greater due to the larger

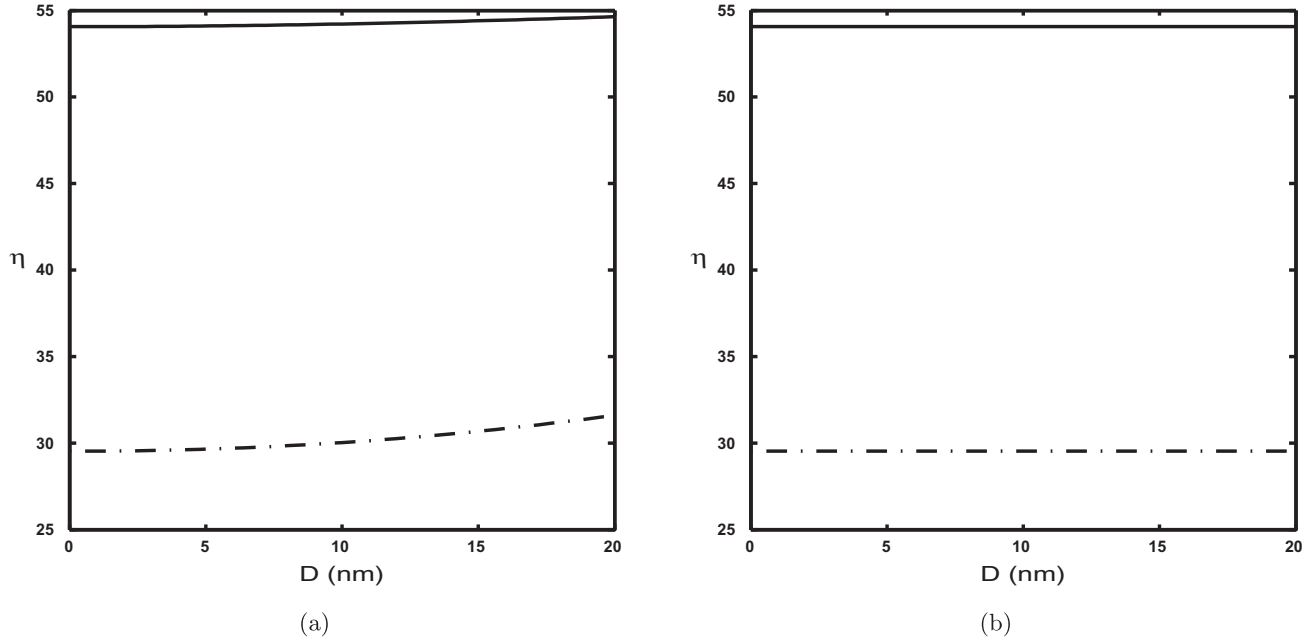

Fig. 9. Efficiency as a function of particle diameter for $\phi = 0.0005$ (dash-dotted line) and $\phi = 0.006$ (solid line). $H = 1.2$ mm and $R = 0.35$. Graph (a) uses the full expression for the nanoparticle extinction efficiency given in (2.17), whilst (b) neglects both Q_s^{np} and the $\mathcal{O}(D^2)$ term in Q_a^{np}.

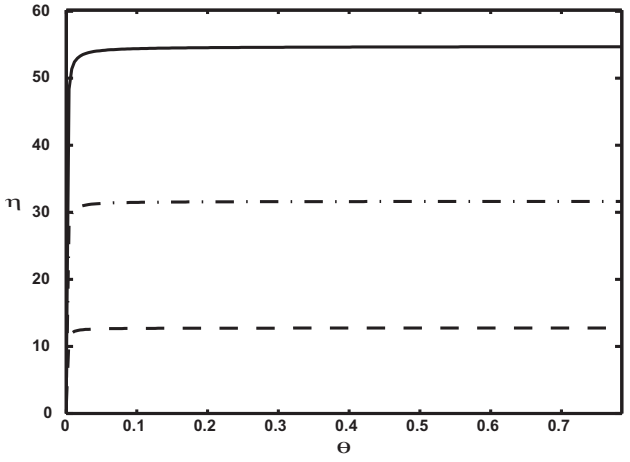

Fig. 10. Efficiency as a function of inclination angle for $\phi = 0$ (dashed line), $\phi = 0.0005$ (dash-dotted line) and $\phi = 0.006$ (solid line). $H = 1.2$ mm and $R = 0.35$.

absorption path. Consequently, the fluid heats up more, resulting in higher temperatures, and thus higher efficiencies. In the case of all three curves, as H continues to increase, η begins to level off. This observation appears to contradict the definition of η in (4.2) which suggests that η depends on $UH \sim H^3$. Hence, one would anticipate η to grow as H increases. However, this H^3 dependence is eliminated upon introduction of the temperature scale ΔT to obtain the reduced efficiency expression (4.3). Thus, the exact relationship between H and η is not obvious as β_0, β_1 and $\overline{T}_0$ are nonlinear functions of H. The numerical simulations of Karami et al. [14] suggest a physical explanation for the levelling off phenomenon. They report that for a collector height of 5 mm, approximately 95% of incoming solar radiation is absorbed by a water-based nanofluid containing single wall carbon nanohorns. Thus, increasing the collector height is advantageous up to point, but beyond this point most of the incoming radiation has been absorbed, and the increase in η is negligible.

Fig. 9 demonstrates the relationship between the particle diameter, D and η. The graphs were obtained using two different definitions for the nanoparticle extinction efficiency, $Q_a^{np} + Q_s^{np}$. The absorption efficiency in (2.17) is composed of a fixed component and a part that varies with α^2, where we recall that α is proportional to D via $\alpha = \pi D/\lambda^*$. The scattering efficiency consists of a single $\mathcal{O}(D^4)$ term. Graph (a) was obtained by using the full expression for the extinction efficiency, and in graph (b) Q_s^{np} and the $\mathcal{O}(D^2)$ term in Q_a^{np} were both neglected. The curves in (a) show that there is a marginal increase in efficiency, whilst efficiency is practically constant in (b). The inclusion of the additional terms in the extinction efficiency is evident by the gradual increase in efficiency in (a). However, since the curves shown in (b) have a similar magnitude to those in (a) it would seem reasonable in general to neglect Q_s^{np} and the $\mathcal{O}(D^2)$ term in Q_a^{np}. In theory, as the particle size increases, and thus the higher order D terms begin to dominate the fixed part, we expect the efficiency to increase rapidly. However, as highlighted, the current model uses the Rayleigh scattering approximation, and is invalid if D becomes sufficiently large. The results in Fig. 9 are consistent with the numerical simulations of Tyagi et al. [33].

Finally, Fig. 10 demonstrates that varying the collector angle of inclination, θ, has an almost negligible effect on the efficiency. This can be explained by noting firstly that from the definition of the average fluid velocity (2.5), $U \sim \theta$. From the efficiency expression (4.2), $\eta \sim U$ and from the temperature rescaling in (3.2) $\Delta T \sim 1/U$. Hence, the variation in η with U, and thus θ, effectively cancels out. This leads to the almost constant curves in Fig. 10.

5. Conclusion

In this paper we have developed a model to determine the temperature variation in a nanofluid-based direct absorption solar collector. The model includes radiative transport and energy equations. A significant problem with previous analytical models has been the evaluation of the wavelength-dependent radiative flux integral which determines the heat source in the energy equation. Previous authors have avoided the problem via simplifications such as treating parameters as being independent of wavelength. Otherwise numerical techniques were employed. In the present

study we included all the wavelength-dependent optical parameters. The radiative flux integral was evaluated numerically and then approximated with a power-law function. Substituting this approximating function into the energy equation then permitted an analytical solution.

The model was written in nondimensional form to show that there are five controlling nondimensional groups, specifically two that describe the heat source, one describing the relative importance of conduction and advection and two describing the heat loss to the surroundings.

The main goal of this work was to develop an analytical understanding of the process and use this to calculate the collector efficiency. In line with previous numerical and experimental studies we found that the collector performance depends strongly on nanoparticle concentration, although there is a limit beyond which it becomes pointless to add more particles (we did not consider the actual cost of the nanoparticles). Similarly efficiency increases with fluid depth. Particle diameter and collector angle had little effect.

Our analytical method used a simplified NDASC model which captured the most important aspects of the problem and gave the correct qualitative behaviour compared to previous studies [25,33]. Several obvious model extensions, outlined here, will be addressed in a future study. As in [31,34], we assumed a constant fluid velocity profile to simplify the energy equation. A more accurate approach is to assume steady laminar flow in the x-direction of the form $u \sim (Hz - z^2)$. The introduction of this seemingly innocuous expression makes the solution method to the heat equation considerably more difficult. The present model, similar to the majority of theoretical and numerical studies from the literature, applies the independent scattering approximation which limits the analysis to $\phi < 0.006$. However, as highlighted, effective collectors can still be obtained even for very low ϕ [30]. We also considered a low-temperature NDASC so that we could assume temperature-independent thermal properties and negligible thermal radiation in the nanofluid. When considering a high-temperature collector one must allow for both of these effects. In the case of thermal radiation our approach is applicable for relatively large temperatures as Veeraragavan et al. [34] note that for temperatures below 750 K radiative emission constitutes for a small fraction of the total radiative heat loss. Finally, we used a simplified approach to allow for reflectance and absorptance in the collector. The reflectance, R, was fixed by comparing our solution with the combined theoretical and experimental treatment of Otanicar et al. [25]. Their model included absorptance and reflectance due to the upper glass panel and the lower surface of the collector which introduces extra wavelength-dependent terms into the boundary conditions.

Conflict of interest

None declared.

Acknowledgements

V. Cregan was supported by a "la Caixa" foundation grant. T. Myers acknowledges the support of a Ministerio de Ciencia e Innovación Grant MTM2011–23789.

References

[1] M. Abdelrahman, P. Fumeaux, P. Suter, Study of solid-gas-suspensions used for direct absorption of concentrated solar radiation, Sol. Energy 22 (1) (1979) 45–48.
[2] D.J. Acheson, Elementary Fluid Dynamics, Oxford University Press, 1990.
[3] R.B. Bird, W.E. Stewart, E.N. Lightfoot, Transport Phenomena, John Wiley & Sons, 2007.
[4] M.Q. Brewster, Thermal Radiative Transfer and Properties, John Wiley & Sons, 1992.
[5] M.Q. Brewster, C.L. Tien, Radiative transfer in packed fluidized beds: dependent versus independent scattering, J. Heat Transfer 104 (1982) 573.
[6] J. Buongiorno, Convective transport in nanofluids, J. Heat Transfer 128 (3) (2006) 240–250.
[7] J. Buongiorno et al., A benchmark study on the thermal conductivity of nanofluids, J. Appl. Phys. 106 (9) (2009). 094312-094312.
[8] S.U.S. Chol, Enhancing thermal conductivity of fluids with nanoparticles, ASME-Publications-Fed 231 (1995) 99–106.
[9] J.A. Eastman, S.U.S. Choi, S. Li, W. Yu, L.J. Thompson, Anomalously increased effective thermal conductivities of ethylene glycol-based nanofluids containing copper nanoparticles, Appl. Phys. Lett. 78 (6) (2001) 718–720.
[10] T. Grosan, I. Pop, Axisymmetric mixed convection boundary layer flow past a vertical cylinder in a nanofluid, Int. J. Heat Mass Transfer 54 (15) (2011) 3139–3145.
[11] Z. Haddad, E. Abu-Nada, H.F. Oztop, A. Mataoui, Natural convection in nanofluids: are the thermophoresis and brownian motion effects significant in nanofluid heat transfer enhancement?, Int J. Therm. Sci. 57 (2012) 152–162.
[12] K.S. Hwang, S.P. Jang, S.U.S. Choi, Flow and convective heat transfer characteristics of water-based Al_2O_3 nanofluids in fully developed laminar flow regime, Int. J. Heat Mass Transfer 52 (1) (2009) 193–199.
[13] S. Kakaç, A. Pramuanjaroenkij, Review of convective heat transfer enhancement with nanofluids, Int. J. Heat Mass Transfer 52 (13) (2009) 3187–3196.
[14] M. Karami, M. Raisee, S. Delfani, Numerical investigation of nanofluid-based solar collectors, IOP Conf. Ser.: Mater. Sci. Eng. 64 (2014) 012044.
[15] C. Kleinstreuer, Y. Feng, Experimental and theoretical studies of nanofluid thermal conductivity enhancement: a review, Nanoscale Res. Lett. 6 (1) (2011) 1–13.
[16] S.M. Ladjevardi, A. Asnaghi, P.S. Izadkhast, A.H. Kashani, Applicability of graphite nanofluids in direct solar energy absorption, Sol. Energy 94 (2013) 327–334.
[17] S.H. Lee, S.P. Jang, Efficiency of a flat-plate solar collector with water-based MWCNT nanofluids, NSTI-Nanotech 2013 (2) (2013) 362–365.
[18] A. Lenert, E.N. Wang, Optimization of nanofluid volumetric receivers for solar thermal energy conversion, Sol. Energy 86 (1) (2012) 253–265.
[19] M.M. MacDevette, T.G. Myers, B. Wetton, Boundary layer analysis and heat transfer of a nanofluid, Microfluid. Nanofluid. (2013) 1–12.
[20] O. Mahian, A. Kianifar, A.S. Kalogirou, I. Pop, S. Wongwises, A review of the applications of nanofluids in solar energy, Int. J. Heat Mass Transfer 57 (2) (2013) 582–594.
[21] J.C. Maxwell, A Treatise on Electricity and Magnetism, vol. 1, Clarendon press, 1881.
[22] J.E. Minardi, H.N. Chuang, Performance of a black liquid flat-plate solar collector, Sol. Energy 17 (3) (1975) 179–183.
[23] T.G. Myers, M.M. MacDevette, H. Ribera, A time-dependent model to determine the thermal conductivity of a nanofluid, J. Nanopart. Res. 15 (7) (2013) 1–11.
[24] T.P. Otanicar, P.E. Phelan, J.S. Golden, Optical properties of liquids for direct absorption solar thermal energy systems, Sol. Energy 83 (7) (2009) 969–977.
[25] T.P. Otanicar, P.E. Phelan, R.S. Prasher, G. Rosengarten, R.A. Taylor, Nanofluid-based direct absorption solar collector, J. Renewable Sustainable Energy 2 (2010) 033102.
[26] H.F. Oztop, E. Abu-Nada, Numerical study of natural convection in partially heated rectangular enclosures filled with nanofluids, Int. J. Heat Fluid Flow 29 (5) (2008) 1326–1336.
[27] A.D. Rakić, Algorithm for the determination of intrinsic optical constants of metal films: application to aluminum, Appl. Opt. 34 (22) (1995) 4755–4767.
[28] W. Roetzel, B. Spang, Typical Values of Overall Heat Transfer Coefficients, VDI Heat Atlas, Springer, 2010. pp. 75–78.
[29] R. Saidur, T.C. Meng, Z. Said, M. Hasanuzzaman, A. Kamyar, Evaluation of the effect of nanofluid-based absorbers on direct solar collector, Int. J. Heat Mass Transfer (2012).
[30] R.A. Taylor, P.E. Phelan, T.P. Otanicar, R. Adrian, R. Prasher, Nanofluid optical property characterization: towards efficient direct absorption solar collectors, Nanoscale Res. Lett. 6 (1) (2011) 1–11.
[31] R.A. Taylor, P.E. Phelan, T.P. Otanicar, C.A. Walker, M. Nguyen, S. Trimble, R. Prasher, Applicability of nanofluids in high flux solar collectors, J. Renewable Sustainable Energy 3 (2011) 023104.
[32] C.L. Tien, Thermal radiation in packed and fluidized beds, Journal of Heat transfer 110 (4B) (1988) 1230–1242.
[33] H. Tyagi, P. Phelan, R. Prasher, Predicted efficiency of a low-temperature nanofluid-based direct absorption solar collector, J. Sol. Energy Eng. 131 (4) (2009).
[34] A. Veeraragavan, A. Lenert, B. Yilbas, S. Al-Dini, E.N. Wang, Analytical model for the design of volumetric solar flow receivers, Int. J. Heat Mass Transfer 55 (4) (2012) 556–564.
[35] T. Yousefi, F. Veysi, E. Shojaeizadeh, S. Zinadini, An experimental investigation on the effect of Al_2O_3 – H_2O nanofluid on the efficiency of flat-plate solar collectors, Renewable Energy 39 (1) (2012) 293–298.